DRAFT VERSION OCTOBER 7, 2011
Preprint typeset using LaTeX style emulateapj v. 11/10/09

MEASURING SIZES OF ULTRA-FAINT DWARF GALAXIES

R. R. MUÑOZ[1,2], N. PADMANABHAN[3,2], & M. GEHA[2,3]

Draft version October 7, 2011

ABSTRACT

The discovery of Ultra-Faint Dwarf (UFD) galaxies in the halo of the Milky Way extends the faint end of the galaxy luminosity function to a few hundred solar luminosities. This extremely low luminosity regime poses a significant challenge for the photometric characterization of these systems. We present a suite of simulations aimed at understanding how different observational choices related to the properties of a low luminosity system impact our ability to determine its true structural parameters such as half-light radius and central surface brightness. We focus on estimating half-light radii (on which mass estimates depend linearly) and find that these numbers can have up to 100% uncertainties when relatively shallow photometric surveys, such as SDSS, are used. Our simulations suggest that to recover structural parameters within 10% or better of their true values: (a) the ratio of the field-of-view to the half-light radius of the satellite must be greater than three, (b) the total number of stars, including background objects should be larger than 1000, and (c) the central to background stellar density ratio must be higher than 20. If one or more of these criteria are not met, the accuracy of the resulting structural parameters can be significantly compromised. In the context of future surveys such as LSST, the latter condition will be closely tied to our ability to remove unresolved background galaxies. Assessing the reliability of measured structural parameters will become increasingly critical as the next generation of deep wide-field surveys detects UFDs beyond the reach of current spectroscopic limits.

Subject headings: galaxies: dwarf, fundamental parameters - Local Group, structure - photometry

1. INTRODUCTION

The structural parameters of galaxies are of fundamental importance. Uncertainties in estimating a galaxy's physical size, central surface brightness, or total luminosity can quickly propagate into other key galactic properties. For example, galaxy mass measurements, based on either the virial theorem or Jeans equation modeling, depend linearly on the galactic radius (e.g., van der Marel et al. 1994; Wolf et al. 2010). While estimating structural properties should be straightforward, practical considerations such as a limited field size or background estimation can make this a complicated problem.

We have entered a new regime in estimating structural parameters with the discovery of Ultra-Faint Dwarf (UFD) galaxies around the Milky Way and M31 (Willman et al. 2005a,b; Zucker et al. 2006a,b; Belokurov et al. 2006, 2007, 2010; Martin et al. 2009). These objects are found via statistical over-densities of resolved stars in the Sloan Digital Sky Survey (SDSS) and other large imaging surveys with the faintest ones having total luminosities of merely $M_V \sim -1.5$, or $300\,L_\odot$ (Martin et al. 2008; Geha et al. 2009; Belokurov et al. 2010). The exact nature of an individual UFD is often debated (is it a star cluster or dark matter-dominated galaxy? is it in dynamical equilibrium?) and structural parameters are an important tool in this assessment. However, at the detection limits of the SDSS, their low total luminosity translates into a few tens to hundreds of individual stars observed as UFD members. In this regime, a few stars can significantly alter the derived size or total luminosity of a given object.

Structural parameters are determined throughout the literature by measuring the surface brightness of a galaxy as a function of radius, and then fitting an analytic function to this profile (e.g., Caon et al. 1993). The surface brightness profile is usually well determined for galaxies based on an integrated light profile, or in the case of nearby luminous ($M_V < -8$) Local Group galaxies, by summing many thousands of stars in concentric annuli (Irwin & Hatzidimitriou 1995). In applying these techniques to the UFD galaxies, shot-noise due to the low number of available stars can produce unreliable results. As an alternative to surface brightness fitting, Martin et al. (2008) determined structural parameters for the Milky Way UFD galaxies using a Maximum Likelihood (ML) method, building on previous work by Kleyna et al. (1998) and Westfall et al. (2006). In this method, a fixed analytic profile is assumed and its free parameters (typically galaxy center, half-light radius, ellipticity, position angle and the background level) are fit simultaneously using all the available stars (see also Sand et al. 2009; Muñoz et al. 2010). This avoids the need to bin or smooth data and should provide more reliable estimates for systems with low number of stars.

There are regimes, however, where even the maximum likelihood method will produce unreliable structural parameters. In this paper, we explore the transition region between the extreme case where only a few member stars of a resolved galaxy are identified and the well measured galaxies as described above. A quantitative understanding of this regime will be of increasing importance since large surveys, such as SkyMapper, Pan-STARRS, DES, and LSST, are predicted to discover many tens to hundreds more low luminosity systems (Tollerud et al. 2008).

Here we perform a representative set of simulations to explore the accuracy of the ML method for structural parameter estimation in cases when the number of stars detected in a galaxy is a few thousand or less. In § 2.1 and § 2.2 we describe the grid of simulated resolved galaxies, and the ML method used to determine structural parameters in these simulations.

[1] Departamento de Astronomía, Universidad de Chile, Casilla 36-D, Santiago, Chile (rmunoz@das.uchile.cl)
[2] Dept. of Astronomy, Yale University, New Haven, CT 06520
[3] Dept. of Physics, Yale University, New Haven, CT 06520

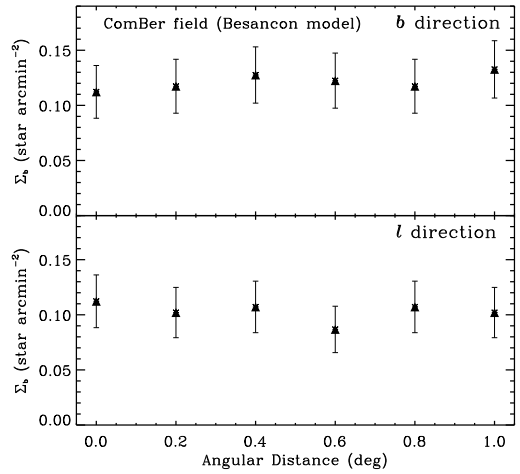

FIG. 1.— Variation of the stellar background density as a function of both Galactic latitude and longitude at the position of the ComBer satellite over a 1° region. These data were simulated using the Besançon Milky Way model. Variations in the background counts are consistent with Poisson noise (error bars).

We then consider parameter optimization for the particular cases of the SDSS and LSST surveys(§ 3), as well as targeted observations with the Canada-France-Hawaii-Telescope (CFHT, § 4). In § 5 we explore the accuracy of the recovered structural parameters split into the separate effects of density contrast, the total number of stars, and the effects of a limited field-of-view (FOV). Finally, in § 6 we summarize our results to distill them into a set of generalized guidelines for future observations.

2. METHODS

How well can structural parameters be measured in the regime where a galaxy is detected as only a low number of resolved stars? To answer this question, we generate a series of simulated UFD galaxies and assess how different observational variables impact our ability to determine their structural parameters. We generate a series of simulated resolved galaxies, varying the total number of stars, the relative density of background stars and the physical size of the object relative to the FOV. We then determine the structural parameters of these systems using a maximum likelihood method and compare our recovered values back to the true inputs.

2.1. *Simulations*

The stellar density profiles of dwarf galaxies, including the UFDs, are typically modeled using analytic density laws such as exponential, Plummer (Plummer 1911) or King (King 1962) profiles. We construct our model galaxies using a Plummer profile, but note that this choice does not affect our conclusions provided the same density law is used to generate both the simulations and recover the structural parameters. The projected Plummer density profile is:

$$\Sigma_{\rm dwarf}(x,y) = \Sigma_0 \left[1 + \left(\frac{(x-x_0)^2+(y-y_0)^2}{R_{1/2}^2}\right)\right]^{-2}, \quad (1)$$

where $R_{1/2}$ is the half-light radius, the galaxy center is at (x_0, y_0) and Σ_0 is the central density. As we are interested in exploring the effects of a limited FOV on the recovered structural parameters, we measure $R_{1/2}$ in units of FOV, L.

TABLE 1
APPROXIMATE VALUE FOR OUR DIFFERENT PARAMETERS FOR THREE REPRESENTATIVE DWARF GALAXIES ASSUMING SDSS AND LSST-LIKE SURVEYS AS WELL AS TARGETED OBSERVATIONS WITH MEGACAM ON THE CFHT. WE ALSO LIST THE ASSUMED r-BAND DEPTHS AND FOVS.

Survey/Telescope	r-band depth	L	$R_{1/2}$	$N_{\rm dwarf}$	N_T [a]	Σ_0
ComBer (M_V = –3.8, $R_{1/2}$ = 6.0′, d = 44 kpc)[b,c]:						
SDSS[c]	22.5	2°	0.05	99	3310	∼ 5
$\rm LSST_{single-exp}$	24	1°	0.1	560	1305	∼ 25
$\rm LSST_{co-added}$	27	1°	0.1	3420	8605	∼ 22
CFHT	24.5	2°	0.05	750	3740	∼ 35
CFHT	24.5	1°	0.1	750	1500	∼ 35
Segue I (M_V = –1.5, $R_{1/2}$ = 4.4′, d = 23 kpc)[c]:						
SDSS[c]	22.5	2°	0.037	65	4340	∼ 3
$\rm LSST_{single-exp}$	24	1°	0.075	200	945	∼ 16
$\rm LSST_{co-added}$	27	1°	0.075	1060	3610	∼ 25
CFHT	24.5	2°	0.037	260	3245	∼ 21
CFHT	24.5	1°	0.075	260	1005	∼ 21
Boo II (M_V = –2.7, $R_{1/2}$ = 4.2′, d = 42 kpc)[c]:						
SDSS[c]	22.5	2°	0.035	37	3940	∼ 3
$\rm LSST_{single-exp}$	24	1°	0.07	210	960	∼ 20
$\rm LSST_{co-added}$	27	1°	0.07	1280	6020	∼ 17
CFHT	24.5	2°	0.035	290	3275	∼ 25
CFHT	24.5	1°	0.07	290	1035	∼ 25

[a] The number of background counts has been derived using background density values taken from Martin et al. (2008) for SDSS and from Muñoz et al. (2010) for the CFHT/MegaCam survey. We note that in general, the latter values are lower than those from SDSS, despite the deeper photometry. For the case of an LSST-like survey we used CMD-filtered counts from the Hubble Ultra Deep Field and assumed that 90% of background galaxies can be removed.
[b] From Muñoz et al. (2010).
[c] From Martin et al. (2008).

Any stellar survey will also include some contaminating sources, either foreground Milky Way stars or unresolved background galaxies. We place our satellites over a homogeneous background density Σ_b with Poisson variations. Throughout this paper, we assume Σ_b = 1 over the relevant area, and report the central density Σ_0 in units of the background density. We have assessed the validity of our assumption of a homogeneous background using both the Besançon model at the Galactic position of Coma Berenices (ComBer) and Boötes II (Boo II), and CFHT imaging of the same UFD galaxies. We find that variations for both datasets, in bins of 12 arcmin across a one degree patch in the simulations and the one degree images, are on the order of 10% and are consistent with Poisson noise (see Figure 1). We conclude that background variations over an area of one degree, relevant for Milky Way UFDs, are not significant and our choice of a homogeneous background, as a first approximation, is justified.

Given the Plummer profile above and assuming circular symmetry, a simulated dwarf galaxy is fully described by three free parameters: $R_{1/2}$, Σ_0 and N_T. The final parameter N_T is the total number of objects, including UFD stars and background detections. In Table 1, we list approximate values for a few representative dwarf galaxies as observed by different instrument/survey combinations.

In Figures 2 and 3 we show a dwarf galaxy simulated under different observing conditions. Figure 2 shows one realization of a satellite resembling the UFD galaxy Boötes II (Boo II, M_V = –2.7, d = 42 kpc) as it would be observed by the CFHT/MegaCam combination down to a magnitude limit of r = 24.5. The galaxy is clearly seen above the background level as a centrally concentrated group of resolved objects. In contrast, Figure 3 shows the same galaxy as observed by the SDSS. Due to the much shallower data, the galaxy is dif-

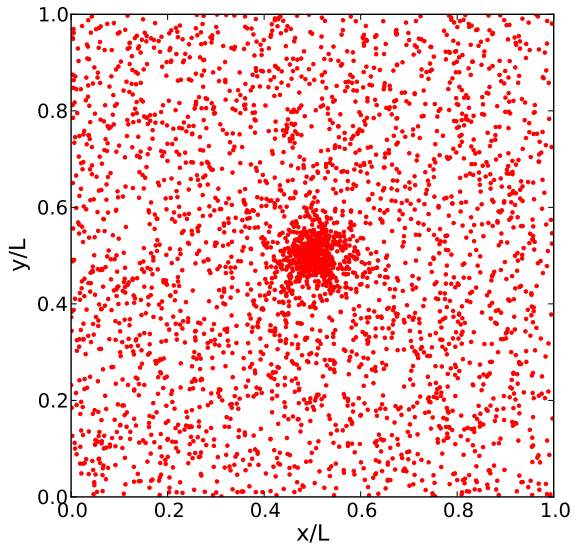

FIG. 2.— Simulated star map of an ultra-faint galaxy with parameters: $R_{1/2} = 0.07$, $\Sigma_0 = 25$ and $N_T \sim 1000$, similar to a Boo II-like satellite observed with the CFHT/MegaCam combination down to a magnitude limit of $r = 24.5$.

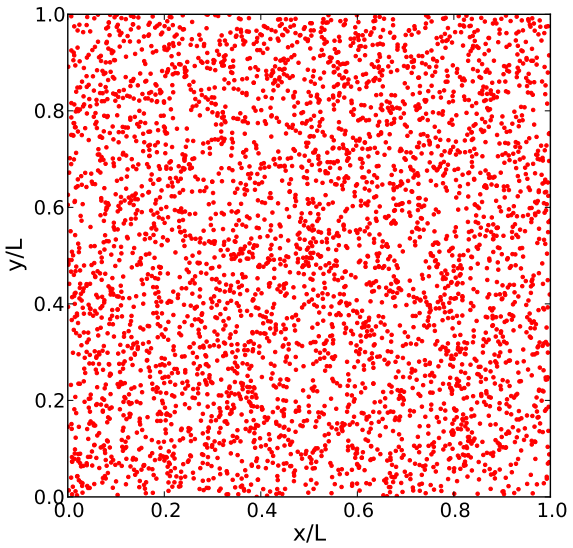

FIG. 3.— Same as Figure 2, but for a Boo II-like satellite as observed in the SDSS. This realization has parameters: $R_{1/2} = 0.035$, $\Sigma_0 = 3$ and $N = 4000$. While the galaxy is not obvious by eye, it is detected as a statistical overdensity of star.

ficult to discern above the background counts. Indeed, the UFD galaxies were only recently discovered because the stellar density contrast between the background and member stars is low– in a typical image a UFD cannot be "seen" without additional filtering of the background.

We run a grid of simulations to cover most of the range of UFD observations presented in Table 1. We vary $R_{1/2}$ between 0.025 and 0.5, Σ_0 from 3 to 100 and the total number of stars N_T from 300 to 5000. For simplicity, the dwarf galaxies are placed at the center of the simulated field.

2.2. *The Maximum Likelihood Method*

We estimate the structural parameters of our simulated galaxies using a maximum likelihood (ML) method. We assume that the stars are distributed according to a density profile,

$$\Sigma(x,y,\mathbf{p}) = \Sigma_{\rm dwarf}(x,y,\mathbf{p}) + \Sigma_b \qquad (2)$$

where $\Sigma_{\rm dwarf}$ is the Plummer profile of equation 1 and Σ_b is an arbitrary background density we choose to normalize to one. The density depends both on the position in the field (x,y) as well as the structural parameters $\mathbf{p} = (R_{1/2}, \Sigma_0, x_0, y_0)$. Note that, in addition to the half light radius and central surface density, we also fit for the central position of the galaxy (x_0, y_0). We continue to assume circular symmetry for simplicity.

The probability $\mathcal{L}_i$ of observing star i is then given by

$$\mathcal{L}_i = \frac{\Sigma(x_i,y_i,\mathbf{p})}{\int_\Omega \Sigma(x,y,\mathbf{p})dx\,dy} \qquad (3)$$

where $\int_\Omega$ is the integral over the observed field and normalizes the probability distribution. The probability of observing the full data set given a particular choice of parameters $\mathbf{p}$ is therefore

$$\mathcal{L} = \prod_i \mathcal{L}_i\,. \qquad (4)$$

The maximum likelihood estimate of the parameters is defined to be the vector $\mathbf{p}$ that maximizes the probability of observing the data. The initial values of the measured parameters were chosen arbitrarily (not at the true value); changing the starting position made no difference to the final results.

Comparing this to previous work (Martin et al. 2008; Sand et al. 2009; Muñoz et al. 2010), we note that the probability is invariant under multiplicative scalings, explicitly justifying our fixing $\Sigma_{\rm b} = 1$. An alternative approach is to explicitly fit for the background density, in which case the normalization integral is then the total number of stars $N_{\rm T}$. This is the approach taken by Martin et al. (2008), although they make a further simplifying assumption that the FOV is large enough that integrating the dwarf profile over the field is equivalent to integrating it to infinity. We do not make this assumption here, since we are also interested in cases where the FOV is comparable to the size of the dwarf.

For each set of free parameters ($R_{1/2}$, Σ_0 and N_T) we run 1000 realizations and generate a distribution for each of the recovered inputs. To assess the quality of the recovered parameters, we report the width of these distributions. We define the quantity $\sigma_{\mathbf{p}}$ as the half width of the central 68% of the distribution. While the distributions are not necessarily Gaussian, this quantity is equivalent to the one-sigma width for a Gaussian distribution. In addition, it is worth mentioning that in all cases, no appreciable bias in the recovered parameters is observed, that is, the observed distribution of measured values is roughly centered on (within at most 10% of) the true input number. In the analysis presented below, we focus primarily on the behavior of the half-light radius and therefore report only $\sigma_{R_{1/2}}$ values.

3. STUDYING UFDS IN WIDE-FIELD IMAGING SURVEYS

In studying UFD galaxies, two different scenarios are relevant: observations made using surveys, and targeted observations with a specific telescope/instrument combination. These two cases present different observational constraints and we examine each separately.

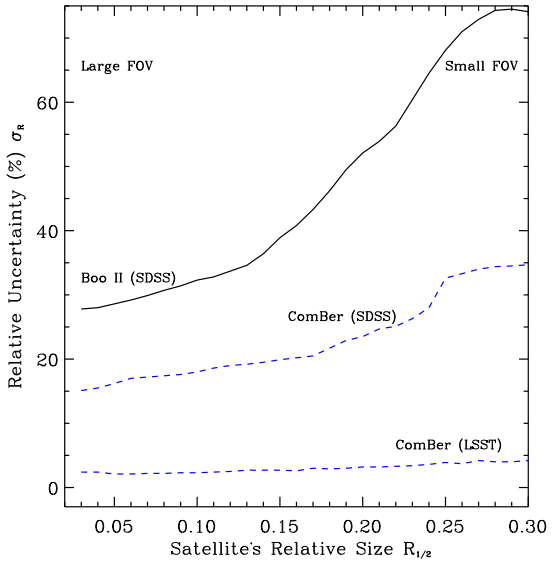

FIG. 4.— Fractional uncertainty $\sigma_{R_{1/2}}$ as a function of the satellite's relative size, $R_{1/2}$ for two UFDs, Boo II (solid lines) and ComBer (dotted lines), "observed" with two photometric surveys, SDSS (upper lines) and LSST (lower line). For each line in this figure, the density contrast has been kept constant and therefore the total number of stars varies from high numbers on the left of the lines to low numbers on the right. This figure shows that when the density contrast is fixed, higher values of $R_{1/2}$ will not necessarily result in better uncertainties because the number of stars decreases rapidly.

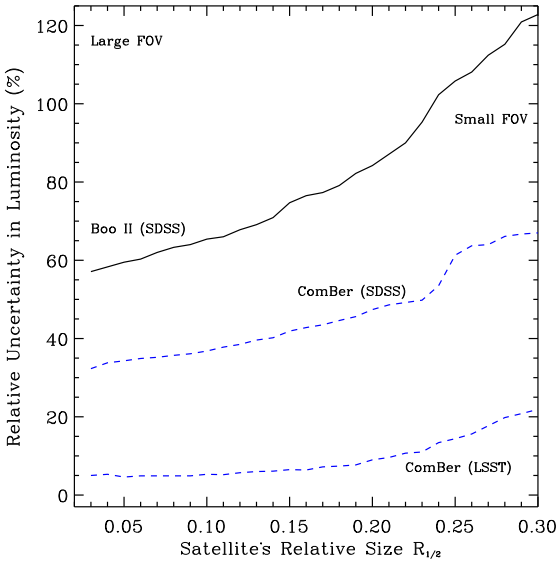

FIG. 5.— Same as Figure 4, but for the fractional uncertainty in luminosity σ_L

All of the UFDs have so far been discovered in the SDSS, but this sample is far from complete due to the survey magnitude limits and sky coverage. Upcoming surveys, such as SkyMapper, Pan-STARRS, DES and LSST, are expected to find many tens to hundreds more satellites (Tollerud et al. 2008). For any wide-field imaging survey two variables pertinent to estimating structural parameters are fixed: the number of observed stars belonging to the dwarf galaxy $N_{\rm dwarf}$, and the density contrast. Both depend on the quality and depth of the photometry. For a given satellite's angular size and distance, the central density depends directly on the number of member stars detected by the survey, and is set primarily by the depth of the photometry, and to a lesser extent, by the quality of the data. The background density increases with the depth of the survey but better quality data allows for more efficient removal of background unresolved galaxies. The only free choice an observer faces is the area around the satellite used to carry out the structural parameter determination. This choice will impact both the relative size of the satellite with respect to the FOV and the total number of stars N_T. Naïvely, one expects the area around the satellite to have a mild effect, if any, on the accuracy of the derived structure, but in the new regime of ultra-faint satellites it is an essential observational consideration.

We focus below on two surveys, SDSS and LSST, and examine how selecting different area sizes affects the accuracy of the measured half-light radii.

3.1. *SDSS*

To illustrate how our simulations can guide the data analysis for study of UFDs, we carry out mock observations for two example dwarf galaxies: Boo II ($M_V = -2.7 \pm 0.9$, $l = 353^\circ.7$, $b = 68^\circ.8$; Martin et al. 2008) and Coma Berenices (ComBer, $M_V = -3.8 \pm 0.6$ $l = 241^\circ.9$, $b = 83^\circ.6$; Muñoz et al. 2010). The former is one of the smallest and faintest of the UFDs, while the latter is rather "typical". We use for reference the structural parameters of Martin et al. (2008) who used SDSS data to carry out a ML study of all UFDs discovered before 2008. For their structural analysis, these authors selected stars within 1 deg radius of each galaxy down to the SDSS magnitude limit of $r \sim 22.5$.

From this catalog, Boo II has a measured half-light radius of $4.2'^{+1.1}_{-1.4}$ and is located at a distance of 42 kpc. In terms of the variables studied by our simulations, this results in $\Sigma_0 \approx 3$, $R_{1/2} = 0.035$ and $N_T = 3940$. The simulations show that this combination of parameters for Boo II yields a $\sigma_{R_{1/2}}$ of roughly 30% (similar to the uncertainty reported by Martin et al. 2008) and a $\sigma_L \sim 90$, indicating that the measurement based on SDSS data is highly inaccurate. It is worth pointing out that Walsh et al. (2008), using deeper photometric observations of Boo II by roughly one magnitude, reported a $R_{1/2} = 2.5' \pm 0.8$, nearly 40% smaller than the $4.2'$ found by Martin et al. (2008), consistent with the uncertainty obtained from our simulations. For the case of ComBer, the results of Martin et al. (2008) give a half-light radius of $6.0' \pm 0.6$ and a distance of 44 kpc, which results in $\Sigma_0 \approx 5$, $R_{1/2} = 0.05$ and $N_T = 3310$. This combination of parameters gives $\sigma_{R_{1/2}} \sim 20\%$ and , $\sigma_L \sim 50$, an improved value as compared to Boo II. In the case of ComBer, the uncertainties reported by Martin et al. (2008) in their measured half-light radii are somewhat lower that those from our simulations. To estimate their errors, these authors assumed that the likelihood function is well-described by a Gaussian distribution near its maximum, an assumption that probably breaks for the fainter objects.

As mentioned above, potential improvements in the accuracy of the measured sizes can only be achieved by changing the area around the satellite used to select UFD member candidates. In particular, we explore the effect of choosing a smaller region. Given that the density contrast will remain constant, using a smaller FOV will bring down the total number of stars. To illustrate the trade-off between increasing $R_{1/2}$ while simultaneously decreasing N_T, in Figure 4 we show the fractional uncertainty as a function of relative size for both Boo II and ComBer when the background density and $N_{\rm dwarf}$ are derived from SDSS (upper lines). In addition, in Figure 5 we show the fractional uncertainty in luminosity,

which roughly correlates with $3 \times \sigma_{R_{1/2}}$ We stress that while the measured uncertainties are shown as function of the satellite's relative size, the total number of stars is also changing. In particular, N_T varies from higher values on the left to lower values on the right. This figure shows that better results are obtained for larger FOV, with the decrease in uncertainty slowly plateauing as the FOV increases. This improvement is a consequence of the increase in the total number of stars (see also §5). In practice however, for regions much larger than those used by Martin et al. (2008) the improvements can be further limited, due to potential background fluctuations and gradients across the field. We therefore conclude that it is not possible to improve substantially the results of Martin et al. (2008) by choosing a smaller FOV. The ultimate limiting factor for a SDSS-like survey is the very low density contrast of the satellites with respect to the background, a reflection of both their low surface brightness and the relatively shallow limit of SDSS, a limitation that can be applied also to SkyMapper, expected to reach a similar depth than SDSS.

In summary, for SDSS-like surveys, our simulations suggest that large FOVs will yield more accurate results, as long as the background density remains homogeneous across the field.

3.2. *LSST*

The Large Synoptic Survey Telescope (LSST) will image the full sky every two nights to a single exposure depth of $r = 24$ over a period of ten years, with a final co-added magnitude limit of $r \sim 27$ (Ivezic et al. 2008). Because LSST is expected to find UFD satellites out to much larger distances as compared to SDSS, the same issues will apply in regard to measuring structural parameters in the limit of low numbers of member stars. An added challenge at LSST magnitude limits will be unresolved background galaxies which will increasingly contribute to the background source counts fainter than $r > 22$ (e.g., see Fig. 1 of Reid & Majewski 1993). To assess the expected performance of LSST we carry out mock observations of the UFD galaxy ComBer, placed at two different distances: its true distance of 44 kpc and farther away at 400 kpc.

We estimate the number of UFD stars, $N_{\rm dwarf}$, detectable down to the full co-added LSST survey magnitude limit using a theoretical luminosity function typical of the UFDs so far discovered: a 13 Gyr old population with overall metallicity of [Fe/H]= –2.27 (Girardi et al. 2004), assuming a Chabrier (2001) initial mass function. For ComBer at 44 kpc, we obtain $N_{\rm dwarf} = 3420$. We combine this information with the known angular size of this system to determine its central density. To derive a density contrast we then need to estimate the background density. For a survey like LSST, this variable is ultimately tied to our ability to characterize the contamination, due either to foreground Milky Way stars or unresolved background galaxies. We estimate the expected contamination from Milky Way stars at these magnitudes by generating fake photometric data for our Galaxy using the TRILEGAL tool (Girardi et al. 2005). For the relevant magnitude range ($22 < r < 27$) this yields foreground star densities that are negligible compared to those of background galaxies within our Color-Magnitude-Diagram (CMD) window[4] (as we illustrate in Figure 6(b)). Our primary contamination will then come from unresolved background galaxies. To estimate their contribution to Σ_b, we use the Hubble-Ultra-Deep-Field (HUDF) catalog under the assumption that the distribution of galaxies is isotropic. Using a region of the CMD similar to the one used to select UFD stars, we estimate a background density of $\Sigma_{\rm gal} = 14.4\,{\rm gal\,arcmin^{-2}}$ down to the limit of $r = 27$. This yields $\Sigma_0 = 2.2/(1-\mu)$, where μ is the fraction of background galaxies that can be potentially removed photometrically. If we assume, for instance, that we can remove 80% of this contamination[5] we obtain $\Sigma_0 \sim 11$. This number may seem surprisingly low compared to the density contrast achieved by Muñoz et al. (2010) using shallower data. However, this is only a reflection of the fact that unresolved galaxy counts grow significantly faster at faint magnitudes. This is true even if we allow the density of background galaxies to vary by a factor a few with respect to the HUDF.

A benefit of deeper photometry is the increase in the total number of detections N_T. For ComBer at 44 kpc, and assuming we can remove 80% of the galaxy counts, we get $N_T = 5050$ for a half-light radius to FOV ratio of 0.25, yielding $\sigma_{R_{1/2}} \sim 4\%$. The lower line in Figure 4 shows the dependence of the relative uncertainty with the satellite's relative size for this particular choice of density contrast value. Both the density contrast and the total number of stars are large enough that the measured uncertainty is rather insensitive to the choice of FOV.

One of the unique aspects of LSST related to UFDs is the expectation of finding galaxies as faint as $M_V = -1$ out to the virial radius of our Galaxy, located roughly at 400 kpc (Tollerud et al. 2008). In Figure 6(a) we show the required fraction of background galaxies that must be removed as a function of r-band depth to achieve a given density contrast in the context of observing a ComBer-like satellite ($M_V = -3.8$, $R_{1/2} = 75$ pc) located at 400 kpc. The figure shows curves for three different values of Σ_0, 15, 20 and 50. To achieve a density contrast of at least 20 for magnitudes fainter than $r = 25$, more than 90% of the unresolved galaxies must be subtracted. We note that while the fraction of galaxies that need to be removed does not increase at deeper magnitudes, the actual background density is a strong function of depth (Figure 6(b)).

Alternatively, one can ask what is the limiting distance at which we can characterize the half-light radii of a given UFD with an intrinsic uncertainty of 10% or better (or equivalently, reach a density contrast of 20 or higher). The answer to this question is ultimately a function of our ability to separate efficiently stellar from non-stellar detections. For illustration purposes, we will assume an upper limit of 90% of galaxy removal[6]. With this number we find that for a ComBer-like satellite, we obtain a density contrast of 20 or more out to about 400 kpc, but not farther. In contrast, for fainter UFDs, i.e. with $M_V \sim -2$, comparable to systems like Segue I, Boo II or Willman I, the limit distance is 200 – 250 kpc. The same is true for brighter ($M_V \sim -5$) but larger UFDs (i.e. systems with half-light radii larger than 100 pc). Achieving density contrasts that allow proper determination of structural parameters for distant UFDs will thus present a major observational challenge.

[4] We define a region around the main sequence of the isochrone described above, located at 44 kpc.

[5] This assumption is based on the results of Muñoz et al. (2010) where we found that using the DAOPHOT morphological parameters χ and sharp, we can remove up to 80% of background galaxies down to a magnitude limit of $r \sim 24.5$. In practice, this fraction is likely to be lower for $r = 27$.

[6] This is in essence an arbitrary number at this time, since we do not know with certainty what will be possible to achieve with LSST, but we deem it a sufficiently challenging upper limit for the purpose of setting a limiting distance.

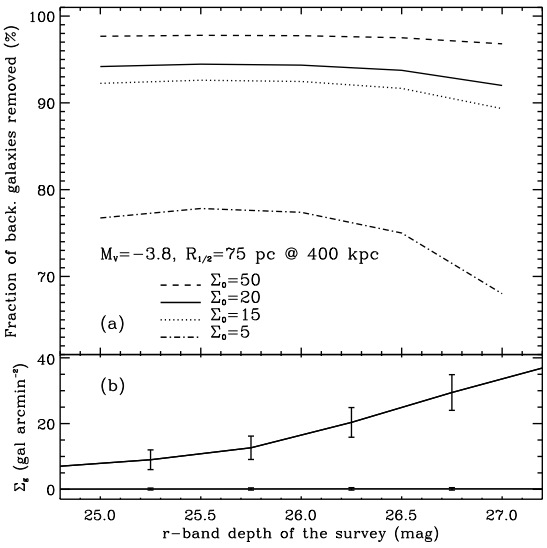

FIG. 6.— *Upper panel:* required fraction of background galaxies that must be removed as a function of *r*-band depth to achieve three different density contrast values: 5, 15, 20 and 50. This particular set of curves represents simulated data for a co-added LSST-like survey of a satellite with absolute magnitude M_V = –3.8, half-light radius of $R_{1/2}$ = 75 pc located at 400 kpc. *Lower panel:* The upper line shows the number density of filtered background galaxies used in panel (a) as a function of *r* magnitude. Galaxy counts were obtained from the HUDF. As a comparison, the lower line shows count densities for Milky Way stars calculated using the TRILEGAL tool.

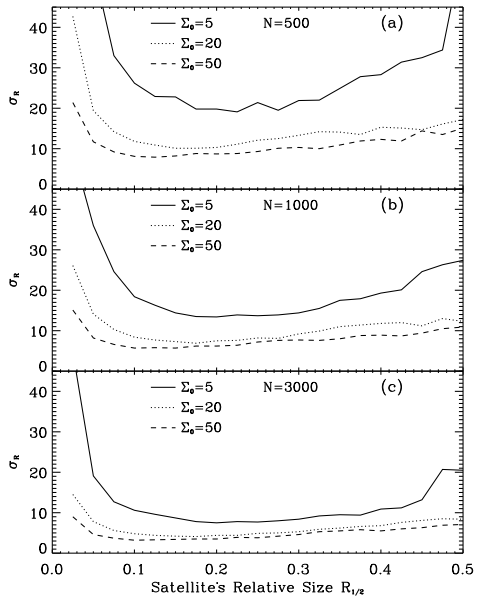

FIG. 7.— Fractional uncertainty $\sigma_{R_{1/2}}$ as a function of the satellite's relative size, $R_{1/2}$. Different panels correspond to different choices of the total number of stars N_T. In each panel, three different density contrasts are shown. This figure shows that (i) density contrasts higher than 20 do not result in a significant improvement in the uncertainty of the measured half-light radii and (ii) the optimal range FOV size is such that $0.1 < R_{1/2} < 0.3$.

4. TARGETED OBSERVATIONS OF UFDS

Follow-up targeted imaging of UFDs can provide more accurate structural parameters than the discovery survey data (Sand et al. 2009; Muñoz et al. 2010). We next explore how to optimize targeted observations to provide the most accurate structural parameter estimates. In contrast to survey data, the practical observing constraint is the total exposure time which translates into a trade-off between photometric depth versus area covered. We choose to analyze a ComBer-like satellite, although the conclusions are applicable to the majority of the UFDs, for two scenarios requiring the same exposure time: a single $1 \times 1\,\mathrm{deg}^2$ pointing down to r = 24.5 and four pointings down to r = 23.0. This choice of area was motivated by Muñoz et al. (2010) who used the telescope/instrument combination of CFHT/MegaCam.

The FOV of the instrument is now fixed, and thus $R_{1/2}$ is determined by the size of the satellite. For observations of ComBer down to $r \sim 24.5$, the extrapolated number of stars belonging to the dwarf galaxy corresponds to $N_{\mathrm{dwarf}} \sim 750$. Assuming a background density similar to that estimated by Muñoz et al. (2010), we obtain $N_T \sim 1500$, $R_{1/2}$ = 0.1 and a density contrast of $\Sigma_0 \sim 35$. Thus, for a single deep pointing covering $1\,\mathrm{deg}^2$ we obtain $\sigma_{R_{1/2}} \sim 5\%$. In comparison, observations down to r = 23 covering twice the size of the FOV (four times the surveyed area), result in $\Sigma_0 \sim 10$, $R_{1/2}$ = 0.05 and $\sigma_{R_{1/2}} \sim 11\%$. This example shows that, in general, given the choice of depth versus area, the former yields better uncertainties. In light of this result, it is relevant to assess whether there is an optimal depth for which uncertainties will be under 10%. Figure 7 shows that, for a given total number of stars and satellite's relative size, the overall uncertainties only marginally improve for density contrasts beyond 20. Thus, in planning targeted observations of UFD galaxies, exposure times should be calculated so that $\Sigma_0 \sim 20$. Deeper photometry, presumably resulting in greater density contrast, will not have an appreciable effect on the overall quality of the measured parameters. Of course, this does not preclude the observer from seeking higher density contrasts for different purposes. In addition, one should plan the area coverage so that, ideally, $0.1 < R_{1/2} < 0.3$ and $N_T > 1000$. Total number of stars as low as N_T = 500 will yield $\sigma_{R_{1/2}} \sim 10-20\%$ within the same range of satellite's relative size and density contrast value (panel (a) of Figure 7).

5. GENERAL TRENDS

The main goal of our simulations is to provide observers with a set of tools to help select the appropriate set of parameters when designing observations of UFDs. As shown in previous sections, the distribution of recovered $R_{1/2}$ values will depend on all three parameters simultaneously: total number of stars, satellite's relative size and density contrast. However, it is possible to distill these results into a set of "rules of thumb" by isolating the effects of each variable independently.

In Figure 8(a) we explore the effects of varying the satellite's relative size. In this figure, we show the distribution of $R_{1/2}$ for three cases where we have varied the size of the satellite. For this particular example we fix N_T = 2000 while simultaneously keeping the density contrast fixed at Σ_0 = 15. The general trend illustrated by panel (a) is such that, for a constant number of stars, in the limit where the size of the satellite is comparable to the FOV ($R_{1/2} \sim 0.5$) or when the field is too large ($R_{1/2} < 0.1$), our ability to recover the intrinsic value of the half-light radii decreases significantly. This is readily understood since for large satellite sizes, with respect to the FOV, we are not able to probe the full profile, while for small sizes, the number of UFD stars decreases (for a fixed N_T) and the satellite's signal is diluted. In practice however, as one uses a larger FOV, the number of stars also increases, and therefore the measured uncertainty behaves as shown in Figure 4, that is, no improvement or worsening in accuracy is

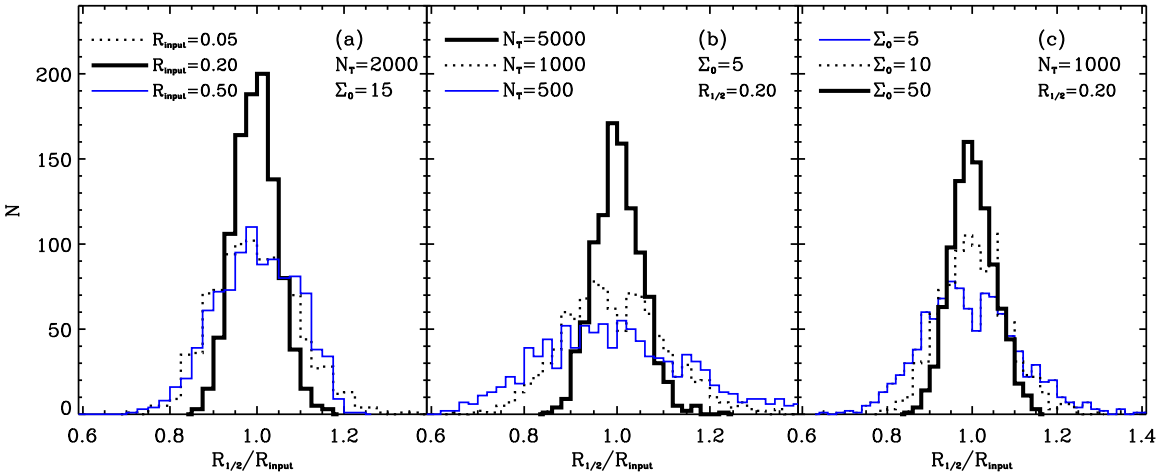

FIG. 8.— Distribution of measured $R_{1/2}$ for simulations where we vary one of the studied variables. *Left panel:* we vary relative sizes. The lowest value of $R_{1/2}$ = 0.05 corresponds to a satellite occupying 10% of the FOV, while the highest value of 0.50 corresponds to a satellite covering the full FOV. *Middle panel:* we vary the total number of stars. The density contrast and satellite's size are kept constant. *Right panel:* we vary the density contrast. The total number of stars has been kept constant at N_T = 1000. and $R_{1/2}$ = 0.2

achieved beyond $R_{1/2} \sim 0.1$. Observing larger FOVs should not be a problem, since one can always use only a subset of the data.

We next investigate the effect of varying the total number of stars, N_T. Figure 8(b) shows the distribution of recovered $R_{1/2}$ for three simulations with input values N_T = 500, 1000 and 5000, bracketing values obtained for various current and future surveys (see Table 1), and constant $\Sigma_0 = 5$ and $R_{1/2} = 0.2$. The figure shows that when all other variables are constant, increasing the total number of stars improves the parameter estimation. For the entire grid of simulations we find that for a wide range of Σ_0 and $R_{1/2}$ values, uncertainties better than 10% require a minimum of N_T = 1000.

Finally, we investigate the effects of varying the density contrast Σ_0, on the recovered half-light radii. In Figure 8(c), we show the distribution of measured half-light radii for three different choices of central density (in units of the background density), 5, 10, and 50 for satellites with $R_{1/2}$ = 0.2 and N_T = 1000. Figure 8 shows that, as intuitively expected, as the stellar density contrast between the satellite and the background increases, the distribution of measured half-light radii becomes narrower and better defined (i.e., more Gaussian) yielding a median value closer to the intrinsic value. We find that for a given combination of N_T and $R_{1/2}$, the improvement in the measured uncertainties is most significant for $\Sigma_0 < 20$. For higher values of the density contrast, $\sigma_{R_{1/2}}$ decreases only marginally.

6. SUMMARY AND CONCLUSIONS

With the discovery of the UFDs we have entered a new luminosity regime dominated by shot noise and where traditional methods to estimate structural parameters no longer yield reliable results. In this article, we have carried out mock observations of a suite of simulated UFD galaxies aimed at exploring how different observational choices impact our ability to extract reliable structural information for these systems. In particular, we have investigated the effects of the total number of stars in a given survey, central-to-background density contrast and relative size of the satellite with respect to the FOV.

Our mock observations allow us to propose a set of simple "rules of thumb" designed to help plan studies of UFDs with existing and/or upcoming surveys as well as plan follow-up observations: (a) the ratio of the radius of the satellite relative to the FOV must be smaller than 0.3, (b) the exposure time should be calculated so that density contrast is ~ 20. Higher numbers will result in marginal gains in parameter uncertainties and (c) for observations of UFDs with photometric surveys the density contrast will be fixed by the survey parameters, and therefore the primary observational choice is the area around the satellite. This should be chosen so that, ideally, $N_T > 1000$.

It is worth keeping in mind that these rules of thumb are derived for the best case scenario, i.e., the choice of density profile faithfully describes the real data, the satellite is perfectly circular, and the background density is homogeneous throughout the FOV. In practice, all three assumptions are likely to be broken in varying degrees, which will lead to further uncertainties not quantified by this study. This leaves room for many possible extensions to the present study. Future work should include, for instance, an exploration of the effects of recovering structural parameters using a density law different from that used to construct the simulations. Including intrinsic elongation for the simulated satellites is also warranted given the high ellipticity found for most UFDs, as it is extending the analysis to satellites that present small tidal disturbances.

We have shown that the new regime of extreme luminosities probed by the UFD population often results in unreliable structural parameters, especially when relatively shallow photometric surveys, such as SDSS, are used. In the particular case of the half-light radii, on which mass estimates depend linearly, numbers based on SDSS catalogs can have intrinsic uncertainties as high as 100% for the faintest and more diffuse UFDs. These higher uncertainties will, for instance, propagate directly into the predicted γ-ray fluxes coming from UFDs due to dark matter annihilation (e.g. Strigari et al. 2008). Assessing the reliability of the measured structural parameters must be regarded as critical in these studies.

We thank an anonymous referee for her/his useful comments. We also thank Beth Willman and Josh Simon for useful discussion on this work. R.R.M. and M.G. gratefully acknowledge support by the National Science Foundation under AST-0908752. M.G. also acknowledges support from the Al-

fred P. Sloan Foundation. R.R.M. acknowledges support from the GEMINI-CONICYT Fund, allocated to the project No. 32080010, and from CONICYT through projects FONDAP No. 15010003 and BASAL PFB-06.

REFERENCES

Belokurov V., et al., 2006, ApJ, 647, L111
Belokurov V., et al., 2007, ApJ, 654, 897
Belokurov V., Walker M. G., Evans N. W., Gilmore G., Irwin M. J., Just D., Koposov S., Mateo M., Olszewski E., Watkins L., Wyrzykowski L., 2010, ApJ, 712, L103
Caon N., Capaccioli M., D'Onofrio M., 1993, MNRAS, 265, 1013
Chabrier G., 2001, ApJ, 554, 1274
Geha M., Willman B., Simon J. D., Strigari L. E., Kirby E. N., Law D. R., Strader J., 2009, ApJ, 692, 1464
Girardi L., Grebel E. K., Odenkirchen M., Chiosi C., 2004, A&A, 422, 205
Girardi L., Groenewegen M. A. T., Hatziminaoglou E., da Costa L., 2005, A&A, 436, 895
Irwin M., Hatzidimitriou D., 1995, MNRAS, 277, 1354
Ivezic Z., Tyson J. A., Allsman R., Andrew J., Angel R., for the LSST Collaboration 2008, arXiv:0805.2366
King I., 1962, AJ, 67, 471
Kleyna J. T., Geller M. J., Kenyon S. J., Kurtz M. J., Thorstensen J. R., 1998, AJ, 115, 2359
Martin N. F., de Jong J. T. A., Rix H.-W., 2008, ApJ, 684, 1075
Martin N. F., McConnachie A. W., Irwin M., Widrow L. M., Ferguson A. M. N., Ibata R. A., Dubinski J., Babul A., Chapman S., Fardal M., Lewis G. F., Navarro J., Rich R. M., 2009, ApJ, 705, 758
Muñoz R. R., Geha M., Willman B., 2010, AJ, 140, 138
Plummer H. C., 1911, MNRAS, 71, 460
Reid N., Majewski S. R., 1993, ApJ, 409, 635
Sand D. J., Olszewski E. W., Willman B., Zaritsky D., Seth A., Harris J., Piatek S., Saha A., 2009, ApJ, 704, 898
Strigari L. E., Koushiappas S. M., Bullock J. S., Kaplinghat M., Simon J. D., Geha M., Willman B., 2008, ApJ, 678, 614
Tollerud E. J., Bullock J. S., Strigari L. E., Willman B., 2008, ApJ, 688, 277
van der Marel R. P., Rix H. W., Carter D., Franx M., White S. D. M., de Zeeuw T., 1994, MNRAS, 268, 521
Walsh S. M., Willman B., Sand D., Harris J., Seth A., Zaritsky D., Jerjen H., 2008, ApJ, 688, 245
Westfall K. B., Majewski S. R., Ostheimer J. C., Frinchaboy P. M., Kunkel W. E., Patterson R. J., Link R., 2006, AJ, 131, 375
Willman B., et al., 2005a, AJ, 129, 2692
Willman B., et al., 2005b, ApJ, 626, L85
Wolf J., Martinez G. D., Bullock J. S., Kaplinghat M., Geha M., Muñoz R. R., Simon J. D., Avedo F. F., 2010, MNRAS, 406, 1220
Zucker D. B., et al., 2006a, ApJ, 650, L41
Zucker D. B., et al., 2006b, ApJ, 643, L103